Development of the Backside Loading Inductive Tactile Force Sensor Using the Flip-Chip Bonding of CMOS Sensing Chip

Sheng-Kai Yeh, Jiunn-Horng Lee, and Weileun Fang, *Fellow, IEEE*

***Abstract*—This study presents a backside loading design inductive tactile sensor with the monolithic integration of thermometer. Based on the commercially available standard complementary metal-oxide-semiconductor (CMOS) process (the TSMC 0.35μm 2P4M CMOS process) and the in-house post CMOS processes, the sensing chip is designed and implemented. The electrical connection is further achieved by using the flip-chip bonding process, and hence the breakage of bonding wires by the tactile load can be avoided. The CMOS sensing chip consists of the magnetic sensing coil and the polysilicon RTD (resistive thermal detector). Moreover, a cavity is defined on the backside (silicon substrate) of CMOS chip to act as a mold for the polymer filler as well as the housing for the chrome steel ball contact interface. The tactile force will cause the polymer deformation and chrome steel ball displacement, and further lead to the magnetic flux change on the sensing coil. Thus, the tactile force is detected by the inductance variation of magnetic sensing coil on the CMOS chip. Moreover, the temperature variation is detected by the resistance change of RTD thermometer, and the in-situ temperature monitoring during tactile loading is achieved. The force response of the proposed tactile sensor and the temperature response of the thermometer have been characterized. The influence of temperature variation on the tactile sensor has also been calibrated. Moreover, the characteristics of the thermometer on sensing chip at different contact conditions are also investigated.**

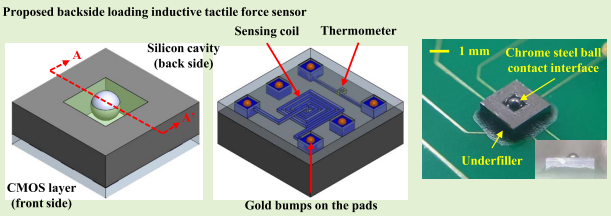

***Index Terms*—Micro tactile sensor, force sensor, touch sensor, inductive sensing, flip-chip bonding, CMOS.**

I. Introduction

TACTILE sensing could provide various information during touch, for instance, the contact loads, the temperature and texture of the contact surface, the hardness of contact object, etc. In addition to image and inertial sensors, the tactile sensors could also serve as the human-machine interface to provide the contact information. Thus, tactile sensors can find applications in various fields such as the industry robots [1], medical tools [2], and consumer products [3], etc. In order to further enhance the applications and performance of tactile sensors, the capability to detect more contact information and the size of sensing units are two critical design considerations. To date, tactile sensors to measure the shear and normal contact forces have been extensively investigated [4]–[17]. Other tactile sensing devices for the detection of fingerprint information [18], surface softness [19], surface roughness [20], and slippage behavior [21] have also been reported. The MEMS (micro-electro-mechanical-systems) technology adopts the semiconductor related micromachining processes to fabricate micro sensors and actuators. Thus, MEMS is a promising technology to reduce the size of tactile sensors. In addition, it is possible to integrate various tactile sensing devices on a single chip using the MEMS technology.

The MEMS tactile sensors have been extensively investigated. The MEMS force sensors with various detection mechanisms, such as the piezoelectric [4], [19], [20], piezo-resistive [5]–[7], [18], capacitive [8]–[11], and inductive [12]–[17], have been developed for tactile sensing applications. In terms of fabrication technologies, the CMOS process is an option to implement tactile sensors [4]–[10], [13]–[17]. The CMOS process with the stacking of multi-layer thin films could enable the electrical routing and the monolithic integration of various sensors and sensing cir-

Manuscript received August 13, 2019; revised October 28, 2019; accepted November 16, 2019. Date of publication November 22, 2019; date of current version February 14, 2020. This work was supported in part by the Ministry of Science and Technology of Taiwan under Grant of MOST 105-2221-E-007-026-MY3, Grant MOST 106-2811-E-007-046-, Grant MOST 107-2622-8-007-005-TE3, and Grant MOST 108-2218-E-007-034-. The associate editor coordinating the review of this article and approving it for publication was Dr. Qiang Wu. *(Corresponding author: Weileun Fang.)*

S.-K. Yeh and W. Fang are with the Power Mechanical Engineering, National Tsing Hua University, Hsinchu 30013, Taiwan, and also with the Institute of NanoEngineering and MicroSystem, National Tsing Hua University, Hsinchu 30013, Taiwan (e-mail: fang@pme.nthu.edu.tw).

J.-H. Lee is with the National Center for High-performance Computing, National Applied Research Laboratories, Hsinchu 30076, Taiwan.

Digital Object Identifier 10.1109/JSEN.2019.2955149

cuits [9], [10], [22], [23]. Presently, micro inductive sensing tactile force sensors with no fragile suspended thin film structures are realized using the CMOS process [13]–[17]. The concerns of process yield and the damage by contact loads can be effectively improved. Moreover, the loads to be detected will contact the surface of the tactile sensing chip. Thus, the damage of fragile electrical routing, such as the wire bonding, becomes another design concern. Two approaches such as the protection of bonding wire using resin [7], [14], [15], [17], [18] and the adoption of flip-chip bonding for electrical connection [10], [11], [16], have been reported to solve this issue.

This study extends the design in [16] to present the flip-chip bonded CMOS inductive tactile force sensor with the loading design at the backside of the substrate. A cavity on the backside of the silicon substrate is prepared after the CMOS process to act as a mold for the polymer filler as well as the housing for the chrome steel ball contact interface [13], [14]. The polymer filler is employed as the deformable mechanical spring and also as the encapsulation material to fix the chrome steel ball. Thus, the external mold employed in [7], [13]–[15], [17] for polymer encapsulation is not required and the device size can be reduced. Moreover, since the chrome steel ball is confined in the cavity on the silicon substrate with encapsulated polymer, it is not easy to be peeled off from the sensing chip [13], [14]. The CMOS process is equipped with multi-layer thin films and this study leverages such advantage to further monolithically integrate other sensing devices on the chip. The integration of the inductive tactile sensor and the thermometer is demonstrated. The sensor performances are characterized and the influence of temperature on sensing results will be investigated. The sensing chip is fabricated by the Taiwan Semiconductor Manufacture Company (TSMC) 0.35 μm 2P4M standard CMOS process together with the in-house post-CMOS processes. This study also exploits the flip-chip bonding approach to replace the wire bonding scheme to avoid the damage of electrical routing by tactile loads.

II. Device Scheme and Illustration

The schematic view of the proposed tactile sensor design is shown in Fig. 1. As depicted in the isotropic illustration in Fig. 1a, a cavity is defined and fabricated on the backside of a chip. By leveraging the characteristics of standard CMOS process platform with multilayer thin films for devices and electrical routings [22], the inductive sensing coil and thermometer are fabricated and monolithically integrated on the chip. Thus, the influence of ambient temperature on the tactile sensor can be calibrated and monitored. The coil for inductance sensing is located at the center of the CMOS chip, and the RTD (resistive thermal detector) thermometer is arranged nearby the sensing coil. Moreover, the symmetric arrangement of the six pads with gold bumps are designed to offer sufficient and balanced support on the chip during the flip-chip bonding. The backside cavity of the CMOS chip is designed to serve as the housing for the polymer filler and chrome steel ball. As shown in Fig. 1b, the polymer filler and chrome steel ball inside the cavity are, respectively, exploited as the spring and contact interface (tactile bump) for the proposed tactile sensor. In this design, the cavity defined on the backside of silicon substrate acts as the mold for polymer filling, and then no additional external mold is required for the definition of the deformable polymer [7], [13]–[15], [17]. Since the cavity could constrain the motion of the chrome steel ball, the assembly of the chrome steel ball becomes easier. Moreover, the cavity could also prevent the detaching of the assembled ball by shear load [13], [14]. The cross-section illustration in Fig. 1b also indicates the flip-chip bonding of the proposed tactile sensor on the PCB (printed circuit board). Note that the tactile load is applied on the chrome steel ball contact interface at the backside of the CMOS sensing chip. The planar magnetic coil on the surface of the CMOS chip is employed for the inductive sensing, and the sensing signal is transmitted through electrical routings on PCB after the flip-chip bonding.

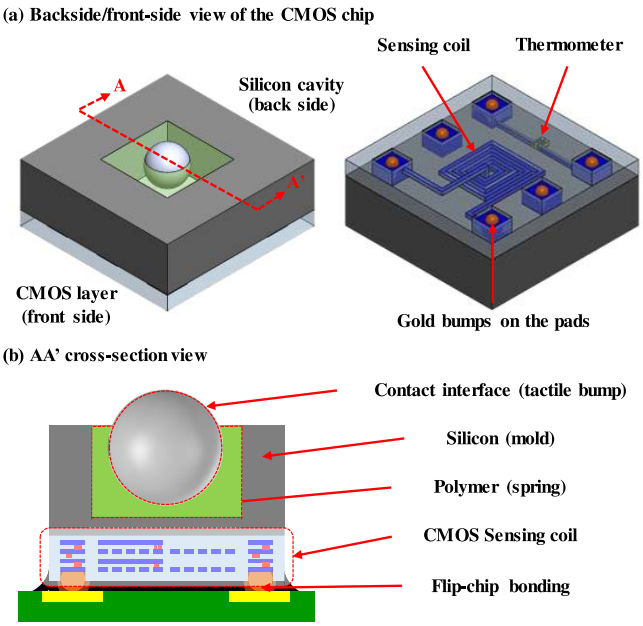

Fig. 1. The structure scheme of the proposed backside loading design tactile sensor composed of the sensing coil and the integrated thermometer on the CMOS chip, gold bumps on the pads, and the backside silicon cavity with the encapsulated chrome steel ball contact interface and the polymer filler, (a) backside/front-side view of the CMOS chip, and (b) AA' cross-section view.

Figure 2 shows the sensing principle of the proposed tactile sensor. As illustrated in Fig. 2a, the chrome steel ball inside the cavity and the sensing coil on the surface of CMOS chip have an initial gap (d_0) and also a corresponding initial inductance (L_0) before applying the tactile load on the proposed sensor. As indicated in Fig. 2b, after the tactile load is applied on the chrome steel ball contact interface, the flexible polymer acting as the spring will be deformed and further causes the displacement of the rigid chrome steel ball. Thus, the gap between the chrome steel ball and the sensing coil is changed from d_0 to d_1, and further causes the inductance change of sensing coil (from L_0 to L_s). According to the inductance

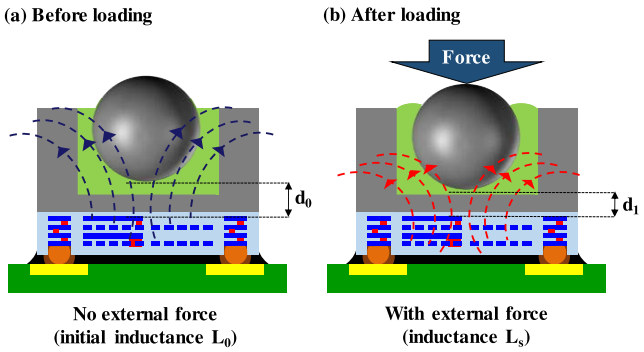

Fig. 2. The sensing principle of the proposed inductive tactile sensor (cross-section of AA' in Fig. 1), (a) the initial inductance of the sensing coil is L_0 before loading, (b) the displacement of the chrome steel ball contact interface caused by the tactile loading will affect the magnetic flux change on the sensing coil and detected by the inductance signal variation (ΔL, L_s-L_0) after loading.

change ΔL detected by the sensing coil, the tactile load can be determined. The finite element simulations (by using the commercial software ANSYS and Ansoft Maxwell) are performed to verify the design concept of the proposed inductive tactile sensor. Figure 3 depicts the typical FEM simulation results. For the load-deflection analysis of ANSYS, the hyperelastic model is employed in the simulation (with Mooney-Rivlin constants $C_{10} = 0.1$ MPa and $C_{01} = 0.0625$ MPa [17]). Moreover, the deformations resulted from normal and lateral loads are simulated by the model. Figures 3a and 3b, respectively, present the predicted polymer deformations induced by the pure normal and pure lateral loads. After that, the deformation results are further substituted into the Ansoft Maxwell to simulate the variation of inductance change with force. The simulation results in Fig. 3c depict the variation of inductance change with the normal force to demonstrate the concept of the present sensor design. Moreover, simulation results in Fig. 3d show inductance changes resulted from lateral forces. This is due to the change of the overlapped region between coil and chrome steel ball when applying a lateral force. However, the results indicate the inductance change induced by pure lateral load is much smaller than that induced by the pure normal load. Moreover, simulation results in Fig. 3e further presents the inductance change of the sensor when under both lateral and normal forces. In this case, the lateral force to cause a maximum deformation (100 μm) in Fig. 3b is used. In comparison, the simulation results for normal loading are also provided in the figure. Simulation results indicate, with the influence of lateral force, the sensitivity of sensor is near 14% lower than the ideal case. Hence, the influence of lateral force is a design concern.

III. Fabrication and Results

Figure 4 depicts the fabrication processes flow of the proposed backside loading design tactile sensor (as shown in the AA' cross-section view of Fig. 1b). As illustrated in Fig. 4a, the standard TSMC 0.35 μm 2P4M (two polysilicon and four metal layers) CMOS process are exploited to fabricate various devices on the CMOS chip. In this study, the sensing coil was implemented using metal layers and the thermometer was

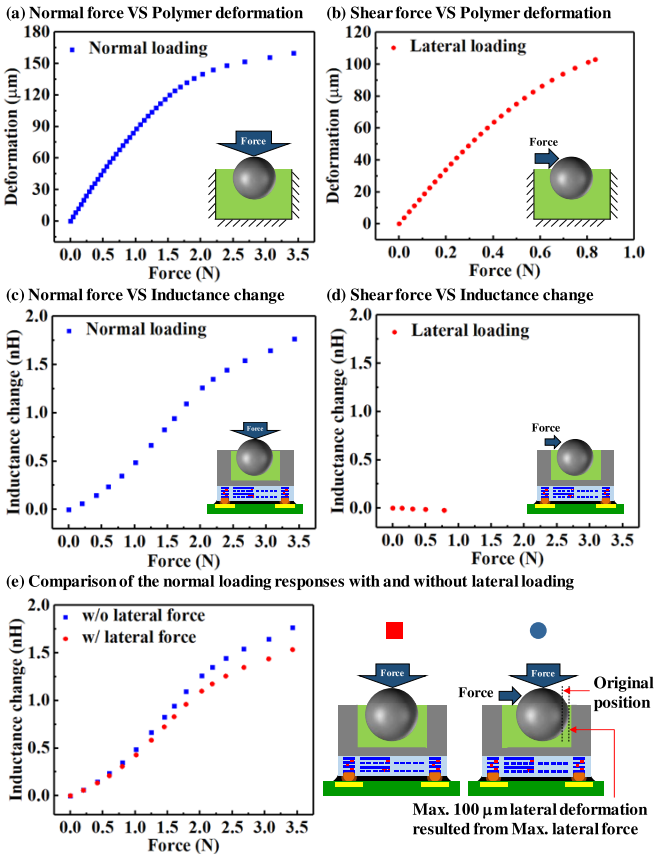

Fig. 3. FEM simulation results, (a-b) different loads VS polymer deformation, (c-d) different loads VS inductance change of the coil, and (e) comparison of the normal loading responses with and without lateral loading.

realized using the polysilicon layer. After the CMOS process, the bonding pads were exposed for signal connection whereas the coil and thermometer were protected by the passivation layer. As shown in Fig. 4b, the backside silicon cavity was defined as the dispensing mold for polymer filler and the housing for the assembly of the chrome steel ball contact interface. The typical depth of the cavity was $\sim$533$\pm$21 μm. Note that after defining the cavity, the remaining substrate thickness (the h_1 indicated in Fig. 4b, in this study it was $\sim$117$\pm$21 μm) needs to provide sufficient stiffness to protect the front-side CMOS layers (total thickness $\sim$7.5 μm). Figures 4c-d show the preliminary in-house flip-chip bonding processes adopted in this study to evaluate the feasibility of the presented device. As depicted in Fig. 4c, the gold bumps were fabricated on pads to form the 3D structure between pads on the CMOS chip and the PCB during the flip-chip bonding process. As shown in Fig. 4d, the flip-chip bonding process was then carried out for the electrical connection by using the silver paste. After curing of the silver paste, the epoxy was exploited as the underfiller to fill the gap between the CMOS chip and the PCB so that the CMOS chip was fixed on the PCB. In this study, the stiff epoxy (WK-8126H) was selected to prevent the remaining silicon substrate (h_1) and the thin front-side CMOS layers from deformation during the tactile loading [24], [25]. After degassing and the curing of the underfiller (with temperature of 120 °C for 2 hour), the polymer (Dow Corning SYLGARD,

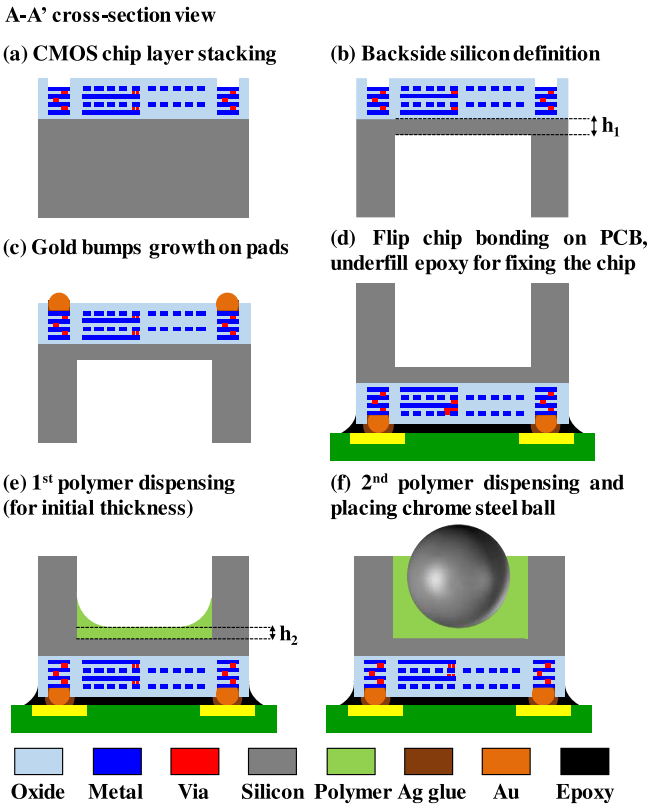

Fig. 4. Fabrication processes of the device, (a) CMOS chip prepared by the TSMC foundry, (b) backside silicon cavity definition, (c) gold bumps growing on the pads of the CMOS chip, (d) flip-chip bonding on the PCB and epoxy underfilling to fix the chip, (e) 1st stage polymer dispensing and curing to define the initial thickness, and (f) 2nd stage polymer dispensing, placing the chrome steel ball and polymer curing.

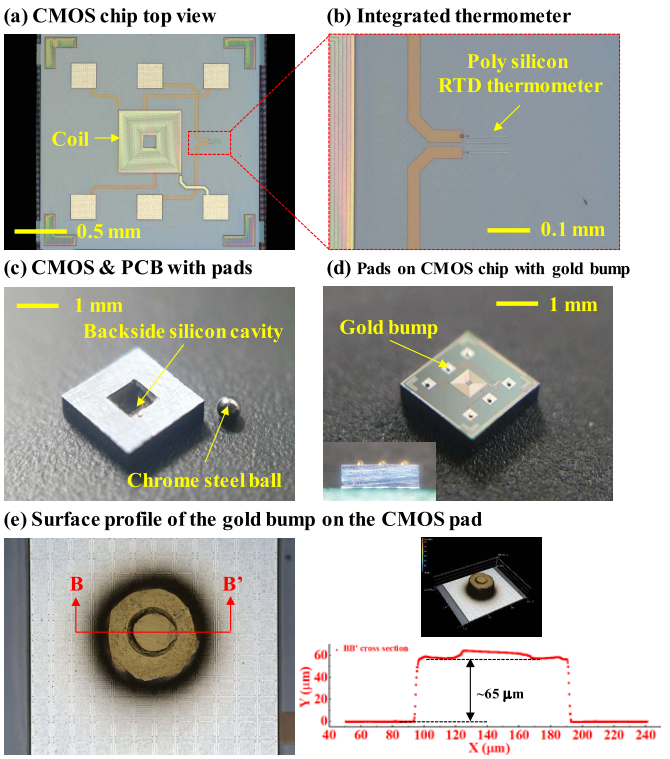

Fig. 5. Typical fabrication results of the chip, (a) top view of the CMOS chip after the fabrication by TSMC foundry (in Fig. 4a), (b) zoom-in caption of the polysilicon thermometer, (c) backside view of the CMOS chip after the silicon cavity definition (in Fig. 4b), (d) bird's eye view and side view of the fabrication result after the definition of the pads growth on the CMOS chip (in Fig. 4c), and (e) surface profile measurement result of the gold bumps on the CMOS chip.

PDMS 184) was dispensed into the silicon cavity by pneumatic dispensing system (Nordson EFD, Ultra 2400 series) to define the initial polymer thickness (h_2 in Fig. 4e), as indicated in Fig. 4e. This is the 1st stage polymer dispensing process, and the thickness of h_2 is $\sim 180 \pm 8$ μm. After the curing of 1st stage polymer (with the temperature of 120 °C for 30 minutes), the polymer was dispensed into the cavity again (the 2nd stage polymer dispensing) and then the chrome steel ball was placed inside the cavity, as illustrated in Fig. 4f. After the curing of the 2nd stage polymer, the chrome steel ball was fixed inside the cavity to complete the fabrication processes.

Figure 5 presents the typical fabrication results of the proposed backside loading tactile sensor. Figure 5a shows the micrograph of the CMOS chip (chip size: 2.2 mm × 2.2 mm) fabricated by the TSMC. The sensing coil, monolithically integrated polysilicon thermometer, and the electrical pads are implemented by the CMOS process. In addition, the six pads (240 μm × 240 μm for each pad) are symmetrically arranged on the chip. The zoom-in micrograph in Fig. 5b further displays the thermometer on the chip, the polysilicon electrical routing of the RTD (resistive thermal detector) can be clearly observed. The micrograph in Fig. 5c shows the backside of the CMOS chip with the silicon cavity after the fabrication process of Fig. 4b, and the chrome steel ball (diameter $\sim$500 μm) before assembly is placed next to the chip. Moreover, Fig. 5d shows the micrograph of the chip with gold bumps on each electrical pad after the fabrication step shown in Fig. 4c. As shown in the cross-section view of inset micrograph, the 3D structure of the gold bump can be clearly observed. The zoom-in micrograph of the gold bump structure is further indicated in Fig. 5e and the surface profile of the 3D structure measured by the laser microscope (Keyence, VK-X1000) indicates that the gold bump has the surface height of $\sim$65 μm and the diameter of $\sim$90 μm. As displayed in the micrograph of Fig. 6a, the CMOS chip is placed next to the bonding pads on PCB for comparison. The alignment marks defined on the PCB are used to align pads on the chip and the PCB during the flip-chip bonding. The micrograph in Fig. 6b presents the side view of the device after the flip-chip bonding process (in Fig. 4d before underfilling process). The cavity at the backside of the CMOS chip and the gap between the CMOS chip and the PCB can be observed. The planar dimension of the cavity is 800 μm × 800 μm to provide sufficient assembly tolerance for the chrome steel ball. Figure 6c displays the CMOS chip adhered to the PCB after the undefilling of epoxy, as the process shown in Fig. 4d. The micrograph in Fig. 6d depicts the final device on PCB (the device under test) after the 2nd polymer dispensing and the chrome steel ball assembly (as shown in Figs. 4e-f). The cross-section view of inset micrograph in Fig. 6d could further display the chrome steel ball fixed by the polymer

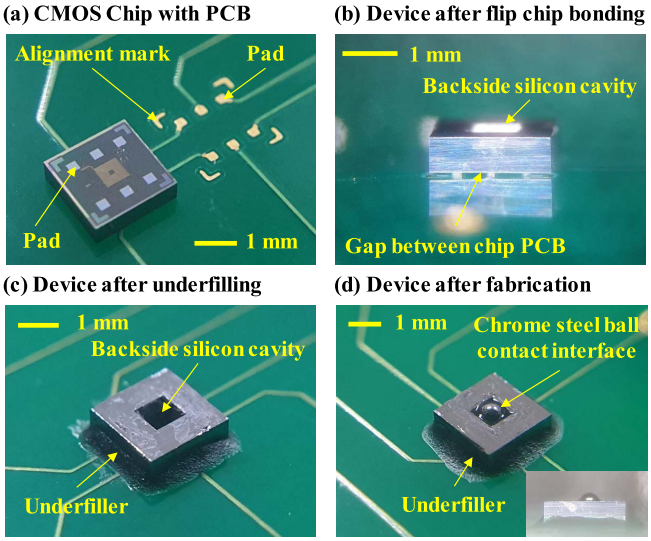

Fig. 6. Typical fabrication results of the chip before/after flip-chip bonding process, (a) the CMOS chip with pads and the PCB with corresponding pads, (b) fabrication result after the flip-chip bonding process before underfilling, (c) result after the underfilling of the epoxy (in Fig. 4d), and (d) result after the polymer dispensing and the assembly of the chrome steel ball contact interface (in Fig. 4f).

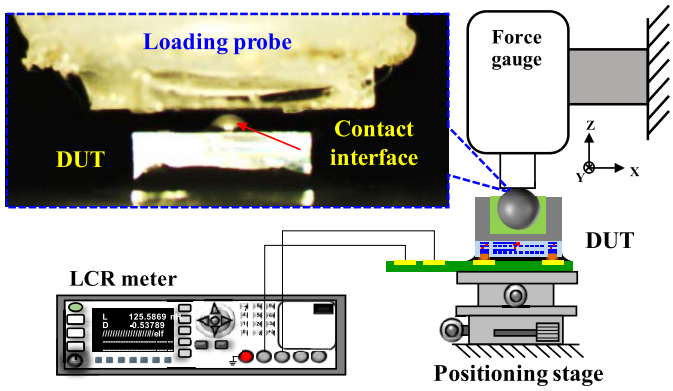

Fig. 7. Measurement setup of the force response of the inductive tactile sensor.

inside the backside silicon cavity and part of the chrome steel ball is above the substrate surface after assembly to serve as the contact interface (tactile bump) of the tactile sensor.

IV. Results and Discussions

In this section, the sensing performances of the backside loading design tactile sensor and the monolithically integrated thermometer would be evaluated. Moreover, the temperature influence of the proposed tactile sensor would also characterized and discussed.

A. Sensor Performances

The measurement setup of the testing system for the tactile sensor is displayed in Fig. 7, the DUT (the device under test shown in Fig. 6d) is mounted on the tri-axial motor positioning stage (Sigma Koki, Z-axis: OSMS80-20ZF-0B, XY-axes: HST-50). The in-plane (XY-axes) positioning stage is used to align the DUT and the commercial force gauge (YOTEC Precision Instrument, FSH-50N). As the out-of-plane displacement is specified by the Z-axis motor stage, the non-conductive acrylic loading probe with glass contact tip (size of 3 mm × 3 mm with thickness of 0.5 mm) on the force gauge will apply a tactile load on the contact interface (chrome steel ball) of the sensor. Meanwhile, the tactile load is monitored and recorded by the force gauge. The inductance changes due to tactile loads are detected by the sensing coil and then transmitted from the PCB to the LCR-meter (Agilent, E4980A). The inset micrograph in Fig. 7 displays the loading probe on the force gauge touching the chrome steel ball contact interface (tactile bump) during the test.

The variation of inductance changes (in the unit of nano-Henry, nH) with tactile loads (in the unit of Newton, N) is recorded using the setup in Fig. 7 to show the force response of the proposed tactile sensor. Figure 8a presents the typical force response measurement results. According to the simulation results in Fig. 3a, the range for applied force is selected as 0∼3 N to prevent the damage of polymer. The measurements indicate the presented tactile sensor has the sensitivity of 1.76 nH/N within the loading range of 0-3 N, which has near 2.75-fold difference as compared with simulation results in Fig. 3c. According to [17], the difference between simulation and experiment results is mainly caused by the deviation of magnetic properties of the chrome steel ball in the simulation model. Note that the inductance change of the sensor will saturate (defined as the turning point in [17]) as the applied force exceeding 3.6 N, and in comparison with the turning point predicted by FEM in Fig. 3 is 2.6 N. According to [17], the difference between simulation and experiment is mainly resulted from the polymer thickness deviation in the simulation model. Moreover, the measured loading and unloading curves in Fig. 8b further depicts the hysteresis characteristic of the presented tactile sensor introduced by the polymer inside the cavity. Since the presented tactile sensor has a monolithically integrated polysilicon temperature sensor, the thermal response of the thermometer is also characterized as shown in the setup in Fig. 9a. Figure 9b shows the calibration curve of the RTD thermometer on the sensing chip. It depicts the measured resistance change (in the unit of ohm) of thermometer varying with the temperature specified by the heater (in the unit of degree of Celsius, °C). The result indicates the RTD thermometer has the sensitivity of 1.4 ohm/°C and the TCR (temperature coefficient of resistance) of 0.06 %/°C within the temperature range of 25-85 °C. In comparison with [26], the polysilicon RTD has a reasonable TCR value.

B. Thermal Influence on the Tactile Sensor

The coefficient of thermal expansion (CTE) of PDMS is 340 ppm/°C [27], and the elastic modulus of PDMS may also vary with the ambient temperature or the contact surface temperature [28]. Thus, the influence of the ambient temperatures on the performances of the presented tactile sensor has been investigated by using the testing setup in Fig. 9a. Measurement in Fig. 10a indicates the chrome steel ball has an out-of-plane (z-axis) displacement of 35 μm caused by

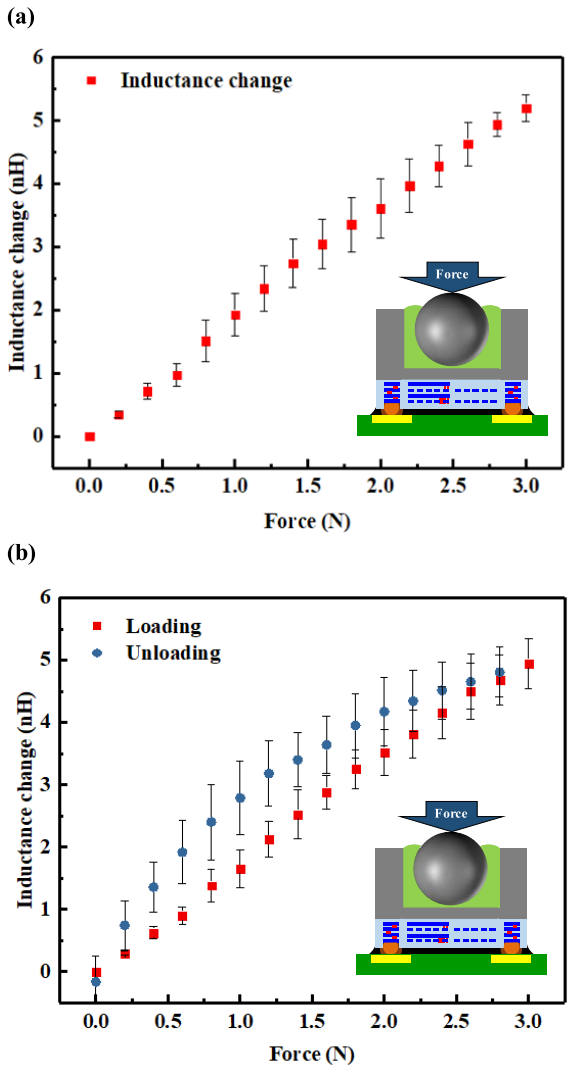

Fig. 8. (a) Force response measurement result of the backside loading design tactile sensor and (b) hysteresis measurement result of the sensor between loading and unloading.

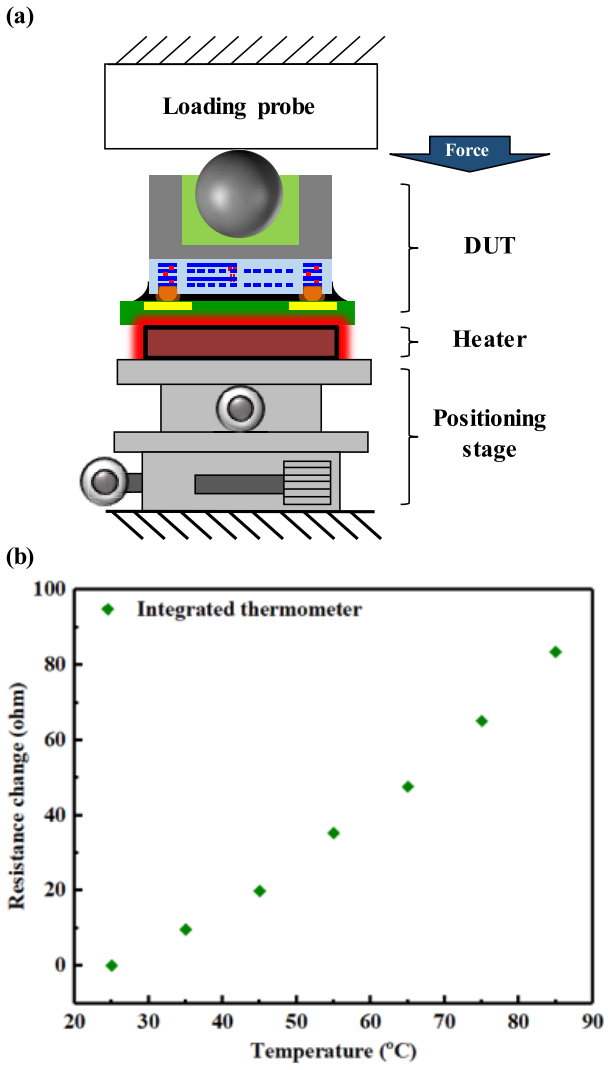

Fig. 9. The measurement result of the integrated thermometer, (a) measurement setup and (b) thermal response calibration result of the thermometer.

the thermal expansion of PDMS as the temperature elevated from 25 °C to 85 °C. Measurements in Fig. 10b further show the PDMS stiffness is near the same as the temperature elevated from 25 °C to 85 °C. Moreover, the force responses under distinct temperatures are characterized. Measurements in Fig. 11a depicts the initial inductance offset under different heating temperatures. The results indicate the initial inductance offset of the presented tactile sensor caused by the thermal expansion of PDMS in Fig. 10a is near -4 % as the temperature elevated from 25°C to 85°C. In addition, measurements in Fig. 11b further show the sensitivity of the tactile sensor is decreased from 1.76 nH/N to 1.57 nH/N as the temperature elevated from 25°C to 85°C. The trend agrees well with the results in Fig. 10a. The measurement results also indicate that the TCS (temperature coefficient of sensitivity) of the proposed tactile sensor is -0.17 %/°C.

This study further establishes the test stand to investigate the characteristics of the thermometer on sensing chip at different contact conditions. As shown in Fig. 12, the commercial hotplate with thermal feedback control (Linkam, TP93) is employed to specify the temperature applied on the chrome steel ball (contact interface) of DUT. The positioning stage could specify a displacement on the hotplate to control the tactile load on the chrome steel ball of DUT. Thus, the test stand could simultaneously specify a tactile load and a temperature on the contact interface of the sensing chip. The DUT is mounted on the force gauge to monitor the tactile load. Finally, the inductance changes due to the tactile load and the resistance change due to the temperature variation are detected by the DUT. Figure 13a shows the temperature difference ΔT between the one specified by hotplate (T_h) and the one measured by the thermometer (T_t) under the loading condition of 1 N. Note that the temperature measured by the thermometer is extracted from the calibration curve shown in Fig. 9b. The temperature difference ΔT is resulted from the low thermal conductance of the PDMS filler. Thus, the temperature difference ΔT is increased as a higher temperature T_h is specified by the hotplate. The results indicate the temperature

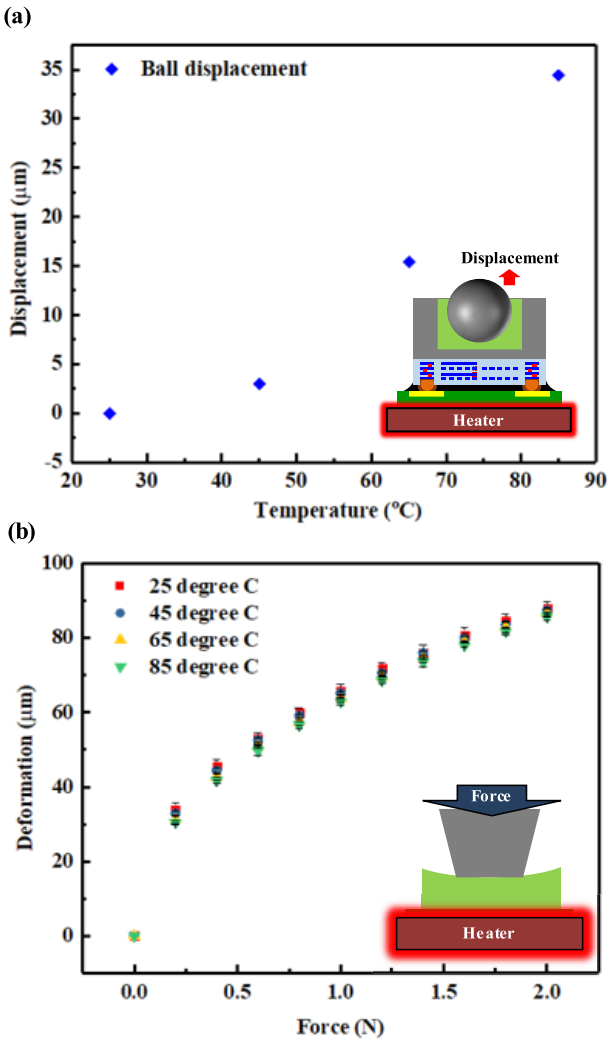

Fig. 10. Thermal influence on the device, (a) out-of-plane displacement of the chrome steel ball under different thermal influences and (b) PDMS stiffness variation under different thermal conditions.

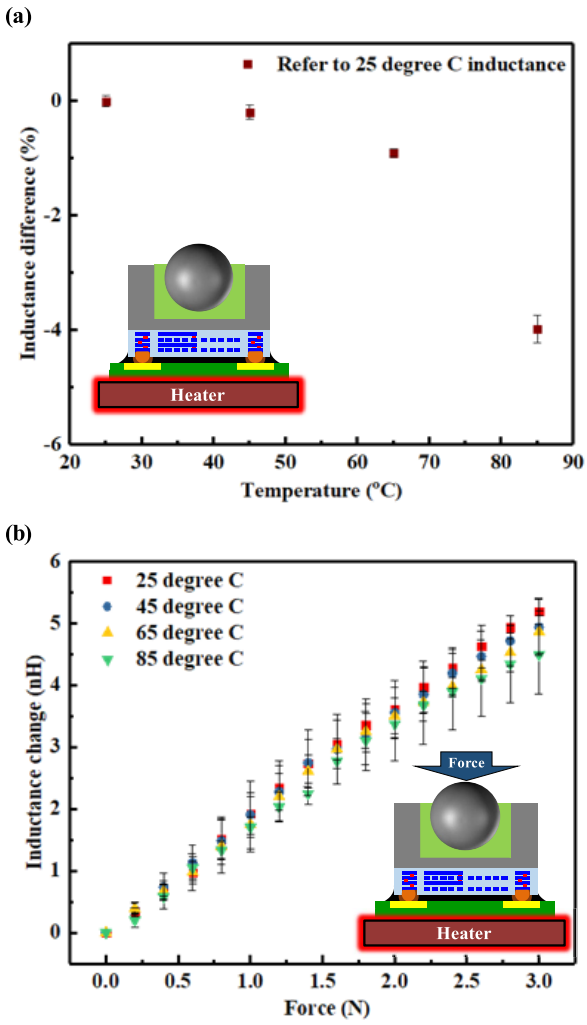

Fig. 11. Thermal influence to the performance of the tactile sensor, (a) initial offset under different thermal conditions and (b) sensitivity drift of the tactile sensor under different thermal conditions.

of contact object measured by the present thermometer has a decrease of ΔT. The polymer filler with larger thermal conductance could reduce the ΔT deviation.

This study also characterizes the thermal response (resistance change versus time) of the thermometer at different tactile loads and contact temperatures. Measurements in Fig. 13b show the resistance changes of the thermometer versus time when specifying three different contact temperatures T_h by hotplate (45 °C, 65 °C, and 85 °C) and also applying three different tactile loads (0.01 N, 0.5 N, and 1 N) on chrome steel ball. Note that the different loading and temperature conditions are denoted as *Load_Temperature*(e.g. 0.01_45 meaning 0.01 N tactile load and 45 °C contact temperature T_h on chrome steel ball through the hotplate, as shown in Fig. 12). The steady-state temperatures T_t extracted from the measured resistance changes of thermometer are also depicted in Fig. 13b. The results indicate the temperature deviation ΔT for the present thermometer is influenced by the tactile load. This is another concern for applications. This study also normalizes the measurements in Fig. 13b with the steady-state

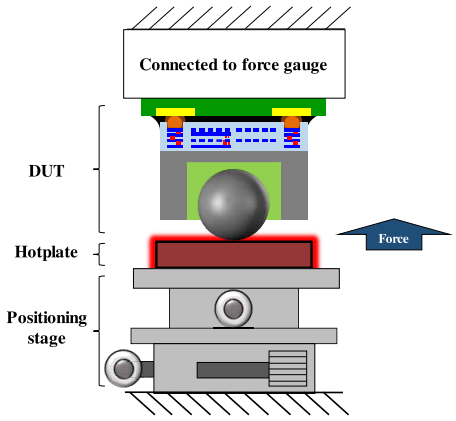

Fig. 12. Measurement setup of the characterization of the thermometer on the sensing chip at different contact conditions.

resistance changes and the results are shown in Fig. 13c. The normalized curves depict the thermal response time (τ_{90}) of the present thermometer is 41±3 s under different loading and temperature conditions. The polymer filler with larger

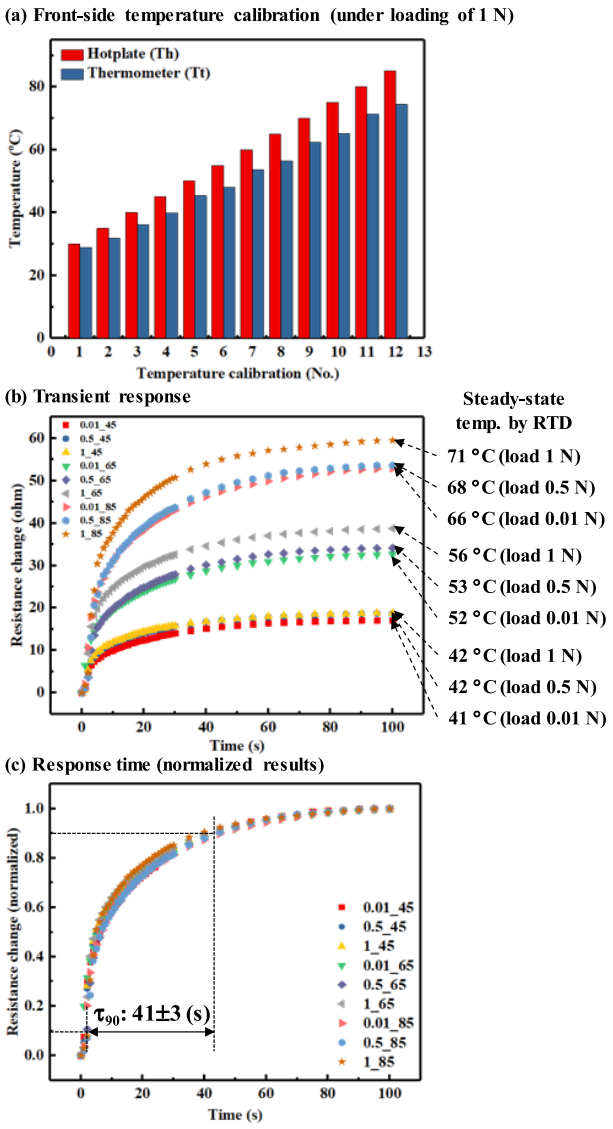

Fig. 13. Measurement results of the thermometer under different contact conditions, (a) temperature calibration result (under 1 N loading) of the hotplate and the thermometer on the sensing chip, (b) thermal response measurement results at different tactile loads and contact temperatures, and (c) normalized measurement results at different tactile loads and contact temperatures (from Fig. 13b).

TABLE I
THE SPECIFICATIONS OF THE PROPOSED DEVICE

Items	Proposed tactile sensor	Unit
Size of sensing coil	600 × 600	μm^2
Size of the device	2.2 × 2.2	mm^2
Size of the tactile bump	0.5	mm
Testing range	0-3	N
Sensitivity (@25 °C)	1.76	nH/N
Temperature coefficient of sensitivity (TCS)	-0.17	%/°C
Items	Integrated thermometer	Unit
Sensitivity (25°C - 85°C)	1.4	Ω/°C
TCR	0.06	%/°C
Response time (contact heat)	41±3*	s

* Averaged by different loading conditions

thermal conductance could reduce the settling time. Finally, Table I summarizes the specifications of the proposed backside loading design inductive tactile sensor.

V. CONCLUSION

In this study, the inductive tactile sensor with monolithic integration of the thermometer is designed and implemented by the TSMC 0.35 μm 2P4M CMOS process and the in-house post CMOS process. A chrome steel ball is assembled in the cavity fabricated at the backside of the silicon substrate by using the polymer filler. The design could reduce the chip height, and also avoid the peel off of the chrome steel ball. Moreover, by leveraging the flip-chip bonding process, the tactile load could apply on the chrome steel ball. Thus, the sensing signals are transmitted through the electrical routings on PCB, and the breakage of bonding wires by the tactile load can be avoided. The CMOS process with the stacking of multilayer thin films enables the monolithic integration of the inductive sensing coil and the RTD thermometer. Hence, the tactile load and the temperature of the contact object can be simultaneously detected. The sensing performances such as the force response of the inductive tactile sensor and temperature sensing of the integrated thermometer are characterized. The influences of the ambient temperature to the tactile sensor including signal initial offset and sensitivity drift are also investigated. The results indicate the initial deformation of the contact interface caused by the thermal expansion of polymer with ambient temperatures is a design concern. Since the polymer filler has been extensively employed in tactile sensors, more detailed investigations on polymer mechanical properties (e.g. viscoelastic phenomenon) are required. It is useful to characterize the response time and the dynamic loading of the presented polymer-based tactile sensor for broad applications. In addition, the thermal responses of the thermometer under distinct contact conditions are measured and discussed. Table I summarizes the specifications of the presented device. Note that the polymer filler with higher thermal conductance can enhance the thermal response time and reduce the temperature deviation between the contact object and the thermometer. For future practical application, the plastic cap adopted in [29] can be added to the fabricated chip through packaging or assembly to constrain the lateral motion of steel ball to reduce the influence of lateral load.

ACKNOWLEDGMENT

The authors would like to appreciate the TSMC and the Taiwan Semiconductor Research Institute (TSRI), for the supporting of CMOS chip manufacturing. They also appreciate the Center for Nanotechnology, Materials Science and Microsystems (CNMM) of National Tsing Hua University for providing the process tools.

REFERENCES

[1] D.-H. Lee, U. Kim, H. Jung, and H. R. Choi, "A capacitive-type novel six-axis force/torque sensor for robotic applications," *IEEE Sensors J.*, vol. 16, no. 8, pp. 2290–2299, Apr. 2015.
[2] P. Puangmali, K. Althoefer, L. D. Seneviratne, D. Murphy, and P. Dasgupta, "State-of-the-art in force and tactile sensing for minimally invasive surgery," *IEEE Sensors J.*, vol. 8, no. 4, pp. 371–381, Apr. 2008.
[3] Y. Shichao and M. A. Walied, "A piezoresistive tactile sensor array for touchscreen panels," *IEEE Sensors J.*, vol. 18, no. 4, pp. 1685–1693, Feb. 2018.

[4] R. S. Dahiya *et al.*, "Towards tactile sensing system on chip for robotic applications," *IEEE Sensors J.*, vol. 11, no. 12, pp. 3216–3226, Dec. 2011.
[5] G. Vásárhelyi *et al.*, "Characterization of an integrable single-crystalline 3-D tactile sensor," *IEEE Sensors J.*, vol. 6, no. 4, pp. 928–934, Aug. 2006.
[6] M. Ádám, T. Mohácsy, P. Jónás, C. Dücso, É. Vázsonyi, and I. Bársonya, "CMOS integrated tactile sensor array by porous Si bulk micromachining," *Sens. Actuators A, Phys.*, vol. 142, no. 1, pp. 192–195, Mar. 2008.
[7] J.-H. Lee, S.-K. Yeh, and W. Fang, "Monolithic/vertical integration of piezo-resistive tactile sensor and inductive proximity sensor using CMOS-MEMS technology," in *Proc. IEEE MEMS*, Seoul, South Korea, Jan. 2019, pp. 826–829.
[8] T. Salo, K. U. Kirstein, T. Vancura, and H. Baltes, "CMOS-based tactile microsensor for medical instrumentation," *IEEE Sensors J.*, vol. 7, no. 2, pp. 258–265, Feb. 2007.
[9] Y.-C. Liu, C.-M. Sun, L.-Y. Lin, M.-H. Tsai, and W. Fang, "Development of a CMOS-based capacitive tactile sensor with adjustable sensing range and sensitivity using polymer fill-in," *J. Microelectromech. Syst.*, vol. 20, no. 1, pp. 119–127, Feb. 2011.
[10] S. Asano *et al.*, "Surface-mountable capacitive tactile sensors with flipped CMOS-diaphragm on a flexible and stretchable bus line," *Sens. Actuators A, Phys.*, vol. 240, pp. 167–176, Apr. 2016.
[11] Y. Hata *et al.*, "Integrated 3-axis tactile sensor using quad-seesaw-electrode structure on platform LSI with through silicon vias," *Sens. Actuators A, Phys.*, vol. 273, pp. 30–41, Apr. 2018.
[12] S. Wattanasarn, K. Noda, K. Matsumoto, and I. Shimoyama, "3D flexible tactile sensor using electromagnetic induction coils," in *Proc. IEEE MEMS*, Paris, France, Jan./Feb. 2012, pp. 488–491.
[13] S.-K. Yeh, H.-C. Chang, and W. Fang, "Development of CMOS MEMS inductive type tactile sensor with the integration of chrome steel ball force interface," *J. Micromech. Microeng.*, vol. 28, no. 4, Feb. 2018, Art. no. 044005.
[14] S.-K. Yeh, H.-C. Chang, C.-E. Lu, and W. Fang, "A CMOS-MEMS electromagnetic-type tactile sensor with polymer-filler and chrome-steel ball sensing interface," in *Proc. IEEE Sensors*, New Delhi, India, Oct. 2018, pp. 1–4.
[15] S.-K. Yeh and W. Fang, "Inductive micro tri-axial tactile sensor using a CMOS chip with a coil array," *IEEE Electron Device Lett.*, vol. 40, no. 4, pp. 620–623, Apr. 2019.
[16] S.-K. Yeh and W. Fang, "Flip-chip integration of inductive CMOS tactile sensor with Si cavity for polymer-filler/metal-ball sensing interface," in *Proc. IEEE MEMS*, Seoul, South Korea, Jan. 2019, pp. 833–836.
[17] S.-K. Yeh, J.-H. Lee, and W. Fang, "On the detection interfaces for inductive type tactile sensors," *Sens. Actuators A, Phys.*, vol. 297, Oct. 2019, Art. no. 111545.
[18] N. Galy, B. Charlot, and B. Courtois, "A full fingerprint verification system for a single-line sweep sensor," *IEEE Sensors J.*, vol. 7, no. 7, pp. 1054–1065, Jul. 2007.
[19] S. Sokhanvar, M. Packirisamy, and J. Dargahi, "MEMS endoscopic tactile sensor: Toward in-situ and in-vivo tissue softness characterization," *IEEE Sensors J.*, vol. 9, no. 12, pp. 1679–1687, Dec. 2009.
[20] W. Liu, P. Yu, C. Gu, X. Cheng, and X. Fu, "Fingertip piezoelectric tactile sensor array for roughness encoding under varying scanning velocity," *IEEE Sensors J.*, vol. 17, no. 21, pp. 6867–6879, Nov. 2017.
[21] Y. Ito, Y. Kim, and G. Obinata, "Robust slippage degree estimation based on reference update of vision-based tactile sensor," *IEEE Sensors J.*, vol. 11, no. 9, pp. 2037–2047, Sep. 2011.
[22] C.-M. Sun, C. Wang, M.-H. Tsai, H.-S. Hsieh, and W. Fang, "Monolithic integration of capacitive sensors using a double-side CMOS MEMS post process," *J. Micromech. Microeng.*, vol. 19, no. 1, Dec. 2008, Art. no. 015023.
[23] S.-C. Chen, V. P. J. Chung, D.-J. Yao, and W. Fang, "Vertically integrated CMOS-MEMS capacitive humidity sensor and a resistive temperature detector for environment application," in *Proc. Transducers*, Kaohsiung, Taiwan, Jun. 2017, pp. 1453–1456.
[24] Z. Zhang and C. P. Wong, "Recent advances in flip-chip underfill: Materials, process, and reliability," *IEEE Trans. Adv. Packag.*, vol. 27, no. 3, pp. 515–524, Aug. 2004.
[25] Y. Y. Ong *et al.*, "Underfill selection, characterization, and reliability study for fine-pitch, large die cu/low-K flip chip package," *IEEE Trans. Compon., Packag., Manuf. Technol.*, vol. 1, no. 3, pp. 279–290, Mar. 2011.
[26] H.-M. Chuang, K.-B. Thei, S.-F. Tsai, and W.-C. Liu, "Temperature-dependent characteristics of polysilicon and diffused resistors," *IEEE Trans. Electron Devices*, vol. 50, no. 5, pp. 1413–1415, May 2003.
[27] Dow Corning Corparation. *SYLGARD 184 Silicone Elastomer Technical Data Sheet*. Accessed: Oct. 22, 2019. [Online]. Available: https://consumer.dow.com/content/dam/dcc/documents/en-us/productdatasheet/11/11-31/11-3184-sylgard-184-elastomer.pdf?iframe=true
[28] F. Schneider, T. Fellner, J. Wilde, and U. Wallrabe, "Mechanical properties of silicones for MEMS," *J. Micromech. Microeng.*, vol. 18, no. 6, Apr. 2008, Art. no. 065008.
[29] *FSS-SMT Series Force Sensor*, Honeywell International, Raleigh, NC, USA, 2014.

Sheng-Kai Yeh was born in Taichung, Taiwan. He received the B.S. degree from the Department of Power Mechanical Engineering, National Tsing Hua University, Taiwan, in 2016 and the M.S. degree from the Department of Power Mechanical Engineering, National Tsing Hua University, in 2017, where he is currently pursuing the Ph.D. degree with the Department of Power Mechanical Engineering. His research interests include design and implementation of the microtactile sensor, contact interface design/integration of the microtactile sensor, and the implementation of CMOS-MEMS sensors.

Jiunn-Horng Lee was born in Kaohsiung, Taiwan. He received the M.S. degree from the Department of Mechanical Engineering, National Cheng-Kung University, Taiwan, in 1991 and the Ph.D. degree from the Institute of Nano-Engineering and MicroSystems, National Tsing Hua University, Taiwan, in 2010. He joined the National Center for High-performance Computing, National Applied Research Laboratories, Taiwan, in 1991, where he is an Associate Researcher. His research interests include computer-aided analysis of MEMS, solid mechanics, and high-performance computing.

Weileun Fang (F'15) was born in Taipei, Taiwan. He received the Ph.D. degree from Carnegie Mellon University, in 1995. His doctoral research focused on the determining of the mechanical properties of thin films using micromachined structures. In 1995, he was a Postdoctoral Research with the Synchrotron Radiation Research Center, Taiwan. He joined the Power Mechanical Engineering Department, National Tsing Hua University, Taiwan, in 1996, where he is a Chair Professor and a Faculty of the NEMS Institute. In 1999, he was a Visiting Associate with Prof. Y.-C. Tai at the California Institute of Technology. His research interests include MEMS with emphasis on microfabrication/packaging technologies, CMOS MEMS, CNT MEMS, microoptical systems, micro sensors and actuators, and characterization of thin-film mechanical properties. Prof. Fang became the IEEE Fellow in 2015 to recognize his contribution in MEMS area. He served as a member of ISC (International Steering Committee) of Transducers from 2009 to 2017, and the ISC Chair from 2017 to 2019. He also served as the General Chair of Transducers Conference in 2017. He was the TPC of IEEE MEMS and EPC of Transducers for many years, and the Program Chair of IEEE Sensors Conference in 2012. He served as the Chief Delegate of Taiwan for the World Micromachine Summit (MMS) from 2008 to 2012, and the General Chair of MMS in 2012. He has close collaboration with MEMS industries and is the VP of MEMS and Sensors Committee of SEMI Taiwan. He is the Chief Editor of JMM, the Associate Editor of the IEEE SENSORS JOURNAL, and the Board Member of the IEEE TRANSACTIONS ON DEVICE AND MATERIALS RELIABILITY.